Electrical studies of single-barrier $Hg_{1-x}Cd_xTe$ heterostructures

D. H. Chow, J. O. McCaldin, A. R. Bonnefoi, and T. C. McGill
T. J. Watson, Sr., Laboratory of Applied Physics, California Institute of Technology, Pasadena, California 91125

I. K. Sou and J. P. Faurie
Department of Physics, University of Illinois at Chicago, Chicago, Illinois 60680

F. A. Shirland and O. K. Wu
Hughes Research Laboratories, Malibu, California 90265

(Received 15 December 1987; accepted 24 February 1988)

We report an experimental study of the electrical properties of single-barrier $Hg_{1-x}Cd_xTe$ heterostructures grown by molecular-beam epitaxy. At high temperature, the measured current is interpreted to be the sum of thermionic and tunneling hole currents. This analysis is applied to data from each of three samples, yielding values of the HgTe–CdTe valence-band discontinuity between 290 ± 50 and 390 ± 75 meV at 300 K. In all three samples, data taken over the range 190–300 K are consistent with a valence-band offset which decreases at lower temperatures. Current–voltage curves are taken at 4.2 K, yielding a novel single-barrier negative differential resistance (NDR) due to electron tunneling. Theoretical simulations indicate that ΔE_v must be < 100 meV at 4.2 K to produce NDR.

I. INTRODUCTION

A number of interesting device applications have been proposed for structures fabricated from thin epitaxial layers of HgTe, CdTe, and $Hg_{1-x}Cd_xTe$.[1–3] In all of these structures, device behavior is strongly tied to the properties of HgTe–CdTe heterojunctions. In particular, the valence-band discontinuity (ΔE_v) at the HgTe–CdTe interface is an extremely important quantity. Considerable disagreement exists in the values of ΔE_v reported to date, which include theoretical studies, x-ray photoemission measurements, magnetoabsorption experiments, and superlattice optical data.[4–15] Electrical studies of single-barrier $Hg_{1-x}Cd_xTe$ heterostructures can provide a fairly direct measurement of ΔE_v. Furthermore, it has been proposed that a novel negative differential resistance mechanism, which relies on electron tunneling across the single barrier, could be observed in this type of heterostructure.[3] A single-barrier negative resistance device might have applications in high-frequency microwave oscillators, amplifiers, and mixers. Although it has been suggested that this effect could be produced in a few material systems,[3,16,17] it has not been previously observed.

II. SAMPLES

In this paper, we report experimental results from three single-barrier $Hg_{1-x}Cd_xTe$ heterostructures grown by molecular-beam epitaxy (MBE). The sample parameters of these structures are summarized in Table I. The compositions of the $Hg_{1-x}Cd_xTe$ layers were obtained by using calibrated growth parameters. Hall-effect measurements were used to determine the electrode carrier concentrations. Sample A was grown on a semi-insulating GaAs substrate in a Riber 2300 system. The active region consisted of a $Hg_{0.05}Cd_{0.95}Te$ barrier layer sandwiched between two $Hg_{0.78}Cd_{0.22}Te$ electrodes. Transmission electron microscopy showed that the $Hg_{0.05}Cd_{0.95}Te$ layer thickness was 180 Å. The $Hg_{0.78}Cd_{0.22}Te$ electrodes were doped n-type with indium, yielding carrier concentrations of 3.6×10^{16} cm^{-3} at 30 K, and 1.5×10^{17} cm^{-3} at 300 K. The top (bottom) electrode was 0.5 μm (3 μm) thick. A 2.5-μm CdTe buffer layer preceded the growth of the active device region of the heterostructure. Samples B and C were grown on CdTe and $Cd_{0.5}Zn_{0.5}Te$ substrates, respectively, in a modified VG V80H II–VI system. In both samples, the active region consisted of a 180-Å $Hg_{0.15}Cd_{0.85}Te$ barrier layer sandwiched between two HgTe electrodes. The HgTe electrodes had intrinsic n-type carrier concentrations of 6×10^{17} cm^{-3} (7×10^{17} cm^{-3}) at room temperature in sample B (C). In both samples, the top (bottom) electrode was 0.5 μm (1 μm) thick, with a 3.3-μm CdTe buffer layer preceding the growth of the active region.

Sample A is a fundamentally different type of single-barrier heterostructure from samples B and C because the $Hg_{0.78}Cd_{0.22}Te$ electrodes in sample A have a nonzero band gap. This difference has two major implications for the I–V behavior expected from the samples. First, the electrode band gap increases the potential barrier to thermionic emission of holes across the structure. Therefore, we expect the high-temperature currents from sample A to be smaller than those from samples B and C. Second, the band gap prevents carriers from tunneling from the valence band of one electrode to the conduction band of the other at low voltages. Since negative differential resistance (NDR) can arise in these structures only when the current is dominated by electron tunneling between the conduction bands of the two electrodes,[3] NDR could be observed in sample A, but probably not in samples B and C.

Circular mesas were fabricated in sample A by wet etching with Br_2:HBr:H_2O in a 0.005:1:3 ratio, and in samples B and C by wet etching with Br_2:ethylene glycol in a 0.002:1 ratio. These chemical etches permitted the use of conventional positive photoresist in photolithographic procedures, as op-

 0734-2101/88/042614-05$01.00

TABLE I. Heterostructure parameters.

Sample	Substrate	Buffer layer	Cladding layer composition	Electrode carrier concentration (cm^{-3})	Barrier composition	Barrier thickness (Å)
A	GaAs	CdTe	$Hg_{0.78}Cd_{0.22}Te$	1.5×10^{17}	$Hg_{0.05}Cd_{0.95}Te$	180
B	CdTe	CdTe	HgTe	6×10^{17}	$Hg_{0.15}Cd_{0.85}Te$	180
C	$Cd_{0.5}Zn_{0.5}Te$	CdTe	HgTe	7×10^{17}	$Hg_{0.15}Cd_{0.85}Te$	180

posed to the more commonly used Br_2:methanol which attacks most positive resists. The two different etch recipes were used because the HgTe cladding layers in samples B and C were etched nonuniformly by the Br_2:HBr:H_2O mixture, with material removed in large flakes. However, the Br_2:ethlylene glycol recipe left a surface which was comparable in quality to the unetched surface. The circular mesas were created with variable size diameters ranging from 35 to 70 μm in sample A, and from 15 to 40 μm in samples B and C. In all three samples, Au was used to make Ohmic contacts to both the tops of the mesas and the etched surface, forming a set of isolated two-terminal devices. Contact resistance tests revealed that the combined series resistance of the contacts, cladding layers, and measurement circuitry was several orders of magnitude less than that of the active device region. Measured currents were found to vary linearly with device area in all three samples, indicating the absence of surface leakage currents.

Current–voltage (I–V) data were taken from all three samples over the temperature range 190–300 K in a low-temperature microprobe station. At these temperatures, the observed current is attributed to the sum of two transport mechanisms: (i) thermionic emission of holes across the barrier layer, and (ii) holes tunneling across a "triangular-shaped" barrier. In addition, I–V measurements were made at 4.2 K in sample A to observe electron tunneling effects. Electrical contacts for these low-temperature measurements were made by attaching thin (20-μm) Au wires to the devices with a conductive epoxy which could be cured at room temperature. This bonding technique was both tedious and time consuming, and resulted in bonds which were not particularly resilient at low temperatures. For some devices, data could not be obtained because the epoxy bonds developed large contact resistances as the sample was cooled. Consequently, only a few devices were studied at 4.2 K.

III. BAND OFFSET MEASUREMENT

A simple theoretical treatment, similar to the Bethe model for Schottky barriers,[18] has been employed to calculate thermionic and tunneling hole current densities across a single barrier as a function of applied voltage.[19] The portion due to thermionic emission, J_{therm} can be written

$$J_{\text{therm}} = A^* T^2 \exp\left(\frac{-\phi + cqV}{kT}\right)\left[1 - \exp\left(\frac{-qV}{kT}\right)\right], \quad (1)$$

where A^* is the modified Richardson constant, ϕ is the potential barrier height, q is the hole charge, and c is the fraction of the total applied voltage which drops across the positively biased electrode. For these heterostructures, A^* is 120 (m_h^*) in A/cm^2 K^2, where m_h^* is the unitless hole mass. The contributions from the light and heavy hole bands are summed to give the total current from this mechanism in sample A. In samples B and C, only the heavy holes contribute to the current significantly, because the light hole band is split off in HgTe. The factor c has been calculated by solving Poisson's equation self-consistently via the method of Bonnefoi *et al.*[20] This method makes the reasonable assumption that the quasi-Fermi level is constant within each electrode. The value of c generally is in the range 0.1–0.4 for the heterostructures studied here, as compared to the case of a Schottky barrier, where $c = 1$.

For sample A, the potential barrier height ϕ in Eq. (1) can be written

$$\phi_{\text{A}} = E_f + E_g^{x=0.22} + (E_v^{x=0.22} - E_v^{x=0.95}), \quad (2)$$

where E_f is the Fermi energy relative to the conduction-band minimum in the electrodes, $E_g^{x=0.22}$ is the energy gap in the electrodes, and the quantity $(E_v^{x=0.22} - E_v^{x=0.95})$ is the valence-band offset at the $Hg_{0.78}Cd_{0.22}Te$–$Hg_{0.05}Cd_{0.95}Te$ interface. This situation is depicted schematically in Fig. 1 of Ref. 19. As discussed previously, ϕ is reduced in samples B and C due to the zero band gap HgTe electrodes:

$$\phi_{\text{B,C}} = E_f + (E_v^{x=0} - E_v^{x=0.85}), \quad (3)$$

where the quantity $(E_v^{x=0} - E_v^{x=0.85})$ is the valence-band discontinuity at the HgTe–$Hg_{0.15}Cd_{0.85}Te$ interface. It should be noted that the reduction in barrier height due to the HgTe cladding layers is partially compensated for by the larger composition difference between the barrier and the electrodes.

For applied voltages of $\sim$50 mV and higher, hole tunneling across the triangular-shaped CdTe barrier makes a contribution to the total current through the heterostructure. This transport mechanism can be treated theoretically in a manner which is analogous to the model for the thermionic hole current. The resulting expression for the hole tunneling current density J_{htun} differs from that for J_{therm} by an integral term which replaces the contribution to ϕ from the valence-band offset. For sample A, we obtain

$$J_{\text{htun}} = A^* T^2 \exp\left(\frac{-E_f - E_g^{x=0.22} + cqV}{kT}\right)\left[1 - \exp\left(\frac{-qV}{kT}\right)\right]\int_0^{u_{\text{A}}} (t^* t) u \exp\left(\frac{-u^2}{2}\right) du. \quad (4)$$

In this expression,

$$u^2/2 = m_h^* v_l^2/kT, \tag{5}$$

where v_l is the group velocity of the holes in the growth direction, $u_A = [2(E_v^{x=0.22} - E_v^{x=0.95})/kT]^{1/2}$, and t^*t is the transmission coefficient for holes tunneling through the CdTe barrier. Similarly, for samples B and C,

$$J_{\text{htun}} = A^*T^2 \exp\left(\frac{-E_f + cqV}{kT}\right)\left[1 - \exp\left(\frac{-qV}{kT}\right)\right] \times \int_0^{u_{B,C}} (t^*t)u \exp\left(\frac{-u^2}{2}\right)du, \tag{6}$$

where $u_{B,C} = [2(E_v^{x=0} - E_v^{x=0.85})/kT]^{1/2}$. In this study, we have calculated t^*t via the Wentzel–Kramers–Brillouin (WKB) method. A two band $k\cdot p$ theory formula[25] was used to find imaginary light hole wave vectors in the CdTe barrier, while imaginary heavy hole wave vectors were determined from the simple "one-band" formula.

Figure 1 contains an experimental current density–voltage (J–V) curve, taken from sample A at 300 K. Also plotted is the J–V curve generated by the theoretical model discussed above for a barrier height $\phi_A = 514$ meV. This value of ϕ_A was chosen by requiring the theoretical and experimental current densities to be equal at 50 mV, and was the only adjustable parameter used. Selecting a different value of the applied bias results in changes in ϕ_A of < 10 meV over the voltage range depicted in Fig. 1. By using the carrier concentration at 300 K, E_f can be estimated to be 44 ± 10 meV above the conduction-band edge in the $Hg_{0.78}Cd_{0.22}Te$ electrodes. The value of $E_g^{x=0.22}$ is taken here to be 185 ± 20 meV at 300 K.[21] In addition, the uncertainty of the cladding layer compositions is estimated to produce an uncertainty of ~ 15 meV in $E_g^{x=0.22}$. Equation (2) then gives $(E_v^{x=0.22} - E_v^{x=0.95}) = 285 \pm 55$ meV. A linear extrapolation of this expression to a pure HgTe–CdTe heterojunction yields $\Delta E_v = 390 \pm 75$ meV.

As discussed previously, samples B and C are expected to yield higher current densities than sample A. Furthermore, the higher electron densities in the pure HgTe electrodes result in less of the applied voltage being dropped there, i.e., the factor c in Eq. (1) is smaller in samples B and C. Thus, the current density varies more slowly with voltage in these samples. Figure 2 contains an experimental J–V curve taken from sample C at 300 K. Also plotted is the theoretical curve generated for a barrier height $\phi_C = 332$ meV, which was selected in the same manner as for sample A. As expected, Fig. 2 displays larger current densities than Fig. 1, and shows a weaker voltage dependence. E_f is estimated to be 75 ± 30 meV for the HgTe cladding layers at 300 K. Equation (3) then gives $(E_v^{x=0} - E_v^{x=0.85}) = 257 \pm 40$ meV. Linear extrapolation of this expression to a pure HgTe–CdTe heterojunction yields $\Delta E_v = 300 \pm 50$ meV. A similar analysis of 300 K data from sample B obtains $\Delta E_v = 290 \pm 50$ meV.

Figure 3 contains the measured current density from each of the three samples as a function of temperature T over the range 190–300 K. The data were taken for an applied bias of 50 mV and are displayed in the standard $\log(J/T^2)$ vs $1/kT$ format, where k is the Boltzmann constant. As discussed previously, the current density in sample A is considerably less than in the other two samples at all temperatures. In addition, samples B and C yield currents with nearly a T^2 temperature dependence, while sample A varies more strongly with temperature. These results can be shown to be consistent with a valence-band discontinuity which decreases nearly linearly as the temperature decreases. In Eq.

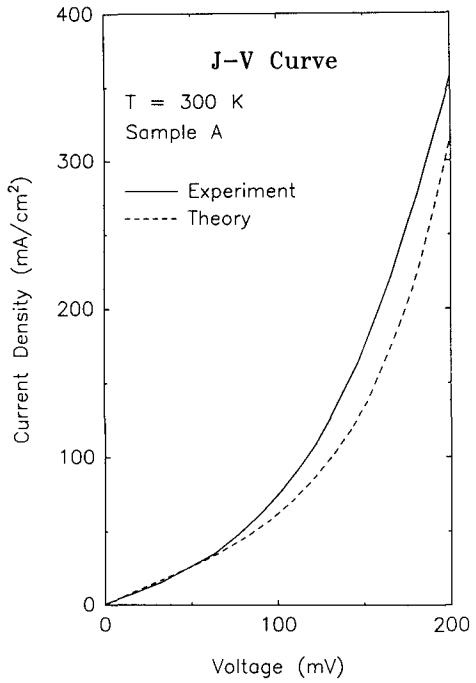

FIG. 1. Experimental J–V curve (—) taken from sample A at 300 K. Also plotted is a theoretical curve calculated for a HgTe–CdTe valence-band offset of 390 meV (– – –). ΔE_v is the only adjustable parameter used to generate the theoretical curve.

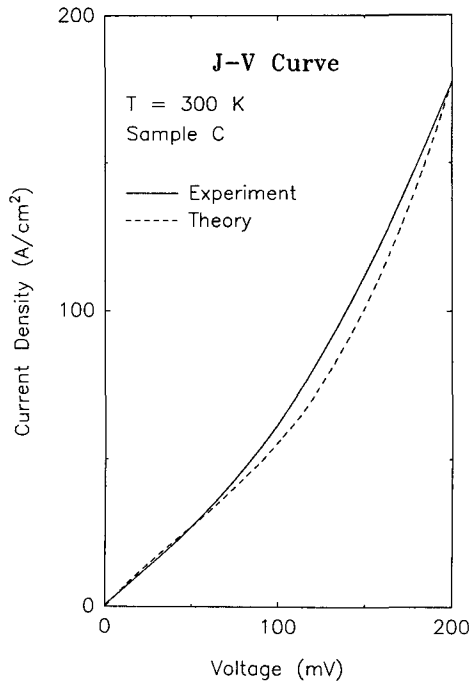

FIG. 2. Experimental J–V curve (—) taken from sample C at 300 K. Also plotted is a theoretical curve calculated for a HgTe–CdTe valence-band offset of 300 meV (– – –).

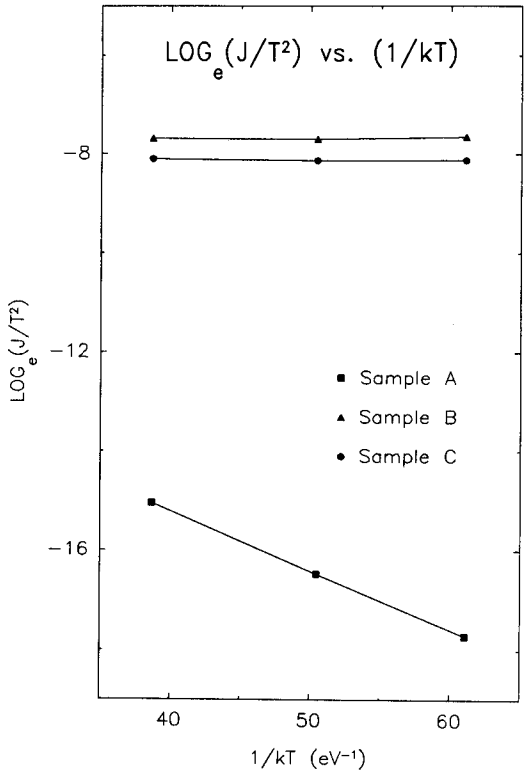

FIG. 3. Measured current density from samples A, B, and C as a function of temperature, plotted in a log(J/T^2) vs $1/kT$ format. The data from all three samples are consistent with a valence-band discontinuity which decreases linearly as the temperature decreases.

(3), E_f behaves roughly as (const$\times T$) due to the nearly intrinsic HgTe cladding layers. Thus, if ($E_v^{x=0} - E_v^{x=0.85}$) also goes as (const$\times T$), $\phi_{B,C}$ will be of this form, and the current density in Eq. (1) will have a T^2 dependence only. On the other hand, Eq. (2) has an extra term, $E_g^{x=0.22}$, which has a temperature independent part[21]:

$$E_g^{x=0.22}(\text{meV}) = 100 + 0.284 \times T. \quad (7)$$

In addition, the Fermi level in sample A is not due to intrinsic carriers, and will therefore have a temperature independent part over the range of interest here. This can be estimated to be 25 meV from the carrier densities given previously. Therefore, we suggest that ϕ_A behaves like 125 meV + const$\times T$. This behavior would give a current density in Eq. (1) which depends on temperature as $[T^2 \times \exp(-125/kT)]$. The line in Fig. 3 has a slope of -120 meV, in reasonably good agreement with this hypothesis. It should be noted that an unknown transport mechanism may be contributing to the observed currents. This could lead to false determinations of the band offsets. However, the fact that the experimental J–V behavior is very close to that predicted by the theoretical model used here supports the assertion that the observed current is due solely to thermionic and tunneling hole currents.

IV. NEGATIVE DIFFERENTIAL RESISTANCE

At $T = 4.2$ K, both the thermionic and tunneling hole transport mechanisms are suppressed. Thus, electron tunneling effects can be observed at this temperature. A calculated band diagram for the heterostructure is displayed in Fig. 1 of Ref. 22. The proposed NDR mechanism is discussed in detail in Ref. 3. The two major theoretical criteria for a single-barrier heterostructure to display NDR are (i) electron tunneling (conduction band) must dominate the current, and (ii) the tunneling electrons must lie closer in energy to the valence-band edge in the barrier material than to the conduction-band edge. Calculations indicate that if ΔE_v is small (< 100 meV), sample A satisfies these conditions adequately. Figure 4 is an experimental I–V curve, taken from a 37-μm-diam device on sample A. The curve displays NDR with a peak current density of 0.51 mA/cm^2 and a peak-to-valley current ratio of 2:1. These results are in reasonable agreement with theoretical simulations which incorporate band bending effects.[20] However, the voltage range over which NDR is displayed is roughly 50 mV higher than that predicted by the theoretical model. NDR was obtained from the device in both bias directions. Other devices tested at 4.2 K gave a variety of results. One device showed NDR in one bias direction only, with a peak-to-valley current ratio of 1.4:1. This device also displayed an inflection (d^2I/dV^2 changed from positive to negative) in the other bias direction. Two other devices showed inflections in both bias directions, but did not have NDR. Finally, three devices did not display any inflections or NDR. In contrast to these results, room-temperature I–V behavior was fairly uniform.[19] It is possible that the electron tunneling currents are far more sensitive to sample nonuniformities than the high-temperature hole mechanisms. Another possible cause of the variations in the I–V behavior of different devices is the poor resiliency of the conductive epoxy bonds at low temperatures. The observation of NDR implies that the valence-band discontinuity at 4.2 K is much smaller than the room-temperature value.

V. SUMMARY

We have reported an electrical investigation of single-barrier $Hg_{1-x}Cd_xTe$ heterostructures grown by MBE. Inter-

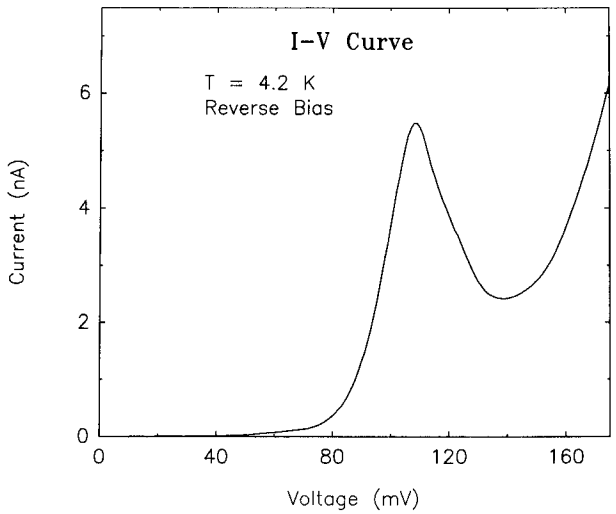

FIG. 4. Experimental I–V curve, taken from sample A at 4.2 K. The curve displays NDR over the voltage range 110–140 mV, with a peak-to-valley current ratio of 2:1.

pretation of the high-temperature currents as thermionic and tunneling hole currents yielded values of ΔE_v between 290 ± 50 and 390 ± 75 meV at 300 K. These results are in reasonable agreement with recent x-ray photoemission measurements.[8–10] The analysis was supported by the experimental J–V behavior, which agreed well with that predicted for the thermionic and tunneling hole mechanisms. In addition, all three samples were found to yield temperature-dependent barrier heights, consistent with $\Delta E_v \propto T$ over the range 190–300 K. Low-temperature (4.2 K) I–V curves from sample A were found to display negative differential resistance due to a novel electron tunneling effect. This is the first reported experimental observation of the single-barrier NDR mechanism. Theoretical simulations indicated that ΔE_v must be < 100 meV at 4.2 K to produce NDR.

ACKNOWLEDGMENTS

We wish to acknowledge S. Nieh for providing us with important TEM data, and O. J. Marsh, T. K. Woodward, and M. B. Johnson for valuable discussions and assistance. This work was supported by the Air Force Office of Scientific Research under Contract No. AFOSR-86-0306 and by the Defense Advanced Research Projects Agency under Contract No. N00014-86-K-0841 and No. F49620-87-C-0021. One of us (D.H.C.) received financial support from International Business Machines Corporation.

[1] J. N. Schulman and T. C. McGill, Appl. Phys. Lett. **34**, 663 (1979).
[2] J. N. Schulman and C. L. Anderson, Appl. Phys. Lett. **48**, 1684 (1986).
[3] D. H. Chow and T. C. McGill, Appl. Phys. Lett. **48**, 1485 (1986).
[4] J. O. McCaldin, T. C. McGill, and C. A. Mead, Phys. Rev. Lett. **36**, 56 (1976).
[5] W. A. Harrison, *Electronic Structure and the Properties of Solids* (Freeman, San Francisco, 1980).
[6] J. Tersoff, J. Vac. Sci. Technol. B **4**, 1066 (1986).
[7] A. Zoryk and M. Jaros, Appl. Phys. Lett. **50**, 1191 (1987).
[8] S. P. Kowalczyk, J. T. Cheung, E. A. Kraut, and R. W. Grant, Phys. Rev. Lett. **56**, 1605 (1986).
[9] T. M. Duc, C. Hsu, and J. P. Faurie, Phys. Rev. Lett. **58**, 1127 (1987).
[10] C. K. Shih and W. E. Spicer, Phys. Rev. Lett. **58**, 2594 (1987).
[11] Y. Guldner, G. Bastard, J. P. Vieren, M. Voos, J. P. Faurie, and A. Million, Phys. Rev. Lett. **51**, 907 (1983).
[12] Z. Yang, M. Dobrowolska, H. Luo, J. K. Furdyna, K. A. Harris, J. W. Cook, and J. F. Schetzina, Superlattices Microstructures (to be published).
[13] J. P. Baukus, A. T. Hunter, O. J. Marsh, C. E. Jones, G. Y. Wu, S. R. Hetzler, T. C. McGill, and J. P. Faurie, J. Vac. Sci. Technol. A **4**, 2110 (1986).
[14] D. J. Leopold, M. L. Wroge, and J. G. Broerman, Appl. Phys. Lett. **50**, 924 (1987).
[15] J. P. Baukus, A. T. Hunter, J. N. Schulman, and J. P. Faurie (unpublished).
[16] G. A. Sai-Halasz, R. Tsu, and L. Esaki, Appl. Phys. Lett. **30**, 651 (1977).
[17] J. Heremans, D. L. Partin, P. D. Dresselhaus, and B. Lax, Appl. Phys. Lett. **48**, 644 (1986).
[18] S. M. Sze, *Physics of Semiconductor Devices* (Wiley, New York, 1981), pp. 255–259.
[19] D. H. Chow, J. O. McCaldin, A. R. Bonnefoi, T. C. McGill, I. K. Sou, and J. P. Faurie, Appl. Phys. Lett. **51**, 2230 (1987).
[20] A. R. Bonnefoi, D. H. Chow, and T. C. McGill, J. Appl. Phys. **62**, 3836 (1987).
[21] R. Dornhaus, G. Nimtz, and B. Schlicht, *Narrow-Gap Semiconductors* (Springer, Berlin, 1983), pp. 158–160.
[22] D. H. Chow, T. C. McGill, I. K. Sou, J. P. Faurie, and C. W. Nieh, Appl. Phys. Lett. **52**, 54 (1988).